_IN ﹣26_

_/). ?.)_

_41 P_

Modelling of Surfaces

Part II–Metallic Alloy Surfaces Using the BFS Method

Guillermo Bozzolo
Analex Corporation
Brook Park, Ohio

John Ferrante
Lewis Research Center
Cleveland, Ohio

and

Robert J. Kobistek
Keithley Instruments
Cleveland, Ohio

July 1994

(NASA-TM-106675) MODELLING OF
SURFACES. PART 2: METALLIC ALLOY
SURFACES USING THE BFS METHOD
(NASA. Lewis Research Center) 41 p

N95-10559

Unclas

G3/26 0017075

Modelling of Surfaces: II. Metallic Alloy Surfaces using the BFS Method

Guillermo Bozzolo

Analex Corporation, 3001 Aerospace Parkway, Brook Park, OH 44142-1003

John Ferrante

National Aeronautics and Space Administration, Lewis Research Center, Cleveland, Ohio 44135

Robert J. Kobistek

Keithley Intruments Inc., 28775 Aurora Rd., Cleveland, OH 44060

Using BFS, a new semiempirical method for alloys, we study the surface structure of fcc ordered binary alloys. We concentrate on the calculation of surface energies and surface relaxations for the $L1_0$ and $L1_2$ ordered structures. Different terminations of the low-index faces are studied. Also, we present results for the interlayer relaxations for planes close to the surface, revealing different relaxations for atoms of different species producing a rippled surface layer.

I. INTRODUCTION

In the last few years, there has been considerable growth in the subject of modelling of materials making use of potent semiempirical methods. These techniques vary in complexity, physical foundation, numerical simplicity and range of applications but overall, they facilitated the development of computational materials science to the level in which it is found today. However, several limitations still exist, and much of the recent work done in this field is directed toward overcoming these difficulties. This problem is more noticeable in the case of alloys: as opposed to the problem of atomic structure of monatomic systems where many techniques, including first-principles approaches, have reached a noticeable degree of sophistication and accuracy, the problem of alloys is, by its own nature, much harder to tackle.

The wealth of experimental studies of surface relaxation on pure metallic surfaces is not matched for alloys [1] However, in spite of the small number of experimental studies [2–4] there seems to be slow but sure progress in the field, as the available theoretical tools for modelling become more accurate. Among them, semiempirical techniques have enjoyed widespread use, helped by the ever-increasing computational capability. In this paper, we will concentrate on one of these approaches, the BFS method [5], which has shown great promise in becoming a viable alternative to deal with the various problems associated with alloys, in that it provides an extremelly simple formalism, a sound physical foundation based on perturbation theory via equivalent crystal theory [6], and a convenient numerical efficiency making it a good candidate for computer simulations of materials properties.

Since its inception two years ago, BFS has been applied to a variety of problems, starting with the basic analysis of bulk properties of solid solutions of fcc [5] and bcc [7] binary alloys (heat of formation [5], lattice parameter [8], etc.) and more specific applications like the energetics of bimetallic tip-sample interactions in an atomic force microscope [9] as well as Monte Carlo simulations of the temperature dependence of surface segregation profiles in Cu-Ni alloys [10]. Other applications include surface structure [11] and a diagramatic

analysis of ordered alloy clusters for the determination of the ground state structure of a given binary alloy [12]. An additional advantage of BFS is that it allows for deriving simple, approximate expressions which describe the trends in segregation as well as elucidating the driving mechanisms for these phenomena [13]. Also, as a consequence of the ideas underlying the foundation of BFS, simple expressions for predicting the composition dependence of bulk alloy properties based solely on pure component properties have been recently derived ('BF rule') [14] providing an alternative to the commonly used Vegard's law [15].

In this paper, we concentrate on the application of BFS to the study of surface structure of metallic alloys. After a detailed description of the method, we present a simple application to the calculation of surface energies, followed by an extensive set of results on the characteristics of surfaces of ordered alloys. These results include an analysis of the surface energies as a function of crystal face, composition of the surface and type of structure, as well as the prediction of the rippling of the surface due to the different relaxations for atoms of different species in mixed-composition surfaces.

II. THE BFS METHOD

A. Basic ideas

We will introduce the BFS formalism [5,7–12,17,13] with reference to the following example. Consider two pure single crystals: one of atomic species A (lattice parameter a_e^A) and one of atomic species B (lattice parameter a_e^B). This will be the *initial* state. The *final* state will be a certain alloy $A - B$ with lattice parameter a_x. The 'ideal' process of alloy formation is shown in Fig. 1 . Let us focus on one of the atoms in the A crystal. Fig. 2 represents the transformation undergone by this atom: there is a change in geometry (the lattice parameter changed from a_e^A to a_x) and a change in composition (some of the neighbors are now B atoms, denoted by dots). In BFS, we approximate this 'ideal' process of alloy formation by a sequence of two independent transformations, as shown in Fig. 3.

In the first transformation, the identity of the atoms is conserved. The atom in question (denoted in figs. 2 and 3 by $\otimes$) sees its environment changed only in terms of the relative distances of the atoms surrounding it. This is a defect that can be straightforwardly treated with any method for monatomic crystals. In particular, because of its effectiveness for dealing with this kind of defects, equivalent crystal theory presents itself as a good candidate for such calculation. In this transformation, the atom in question suffers a change in energy ε^S, which we will call *strain* energy, because it is related only to lattice deformations.

In the second transformation (fig. 3.b), the geometry of the equilibrium crystal is conserved. The atom in question sees its environment changed only in terms of the identity of its neighbors. For evaluating this change in energy, which we will call *chemical* energy, we assume that the neighbors are located in *equilibrium* lattice sites. A change in coordination in the alloy (for example, atoms close to a vacancy or to a surface) would introduce structural information in the chemical energy which, as mentioned above, should be accounted for only by the strain energy term. Therefore, we need to reference the chemical energy so computed to a similar situation where the neighbors of the atom in question are forced to

4

have the same chemical identity. This way, the chemical energy will only carry information on the chemical interaction between atoms of different species, regardless of the geometrical distribution or coordination.

B. Formalism

Adding the strain and chemical energy contributions for a given atom yields the net contribution of this atom to the energy necessary to assemble the alloy $A - B$ from its pure components, which is precisely the heat of formation. Therefore, the contribution of atom i of atomic species X $(X = A, B, ...)$ to the heat of formation of the alloy is

$$\varepsilon_i = \varepsilon_i^S + (\varepsilon_i^C - \varepsilon_i^{C_0}).$$ (1)

where $\varepsilon_i^{C_0}$ denotes the reference to the chemical energy. The total heat of formation , ΔH, is just the sum of the individual contributions of each atom in the alloy. In writing eq.(1) we assume that the two transformations provide a good representation of the process of alloy formation. However, due to the nature of these transformations (i.e., in the calculation of the structural energy we 'freeze' the chemical composition and in the calculation of the chemical energy we 'freeze' the atomic locations), the chemical energy is a constant, solely dependent on the chemical composition of the alloy, which is clearly unrealistic for some situations. One would therefore expect eq.(1) to be a good representation of the alloy for those cases where either there is a small lattice mismatch between the pure components or when the defect represents a small departure from equilibrium. For those cases where such conditions are not met, it is necessary to 'recouple' the two independent processes described above, weighing the chemical contribution to the heat of formation accordingly. In order to accomplish for this, we then introduce a factor which accounts for the asymptotic behavior of the enthalpies of formation of alloys. To be defined later, this 'glue' factor, g_i, links the strain and chemical contributions not only providing a better description of the alloy formation process by recoupling the strain and chemical contributions, but also by giving

5

the correct behavior for large interatomic distances. For alloys of elements with small lattice mismatch, this term is of little relevance in the region of interest, when the typical distances in the alloy are comparable to the distances in the equilibrium crystals. We then rewrite eq.(1) as

$$\varepsilon_i = \varepsilon_i^S + g_i(\varepsilon_i^C - \varepsilon_i^{C_0}).$$

(2)

The strain energy, being that it arises from a single-component system can be written as

$$\varepsilon_i^S = E_C^{(i)} F^*(a_i^{S*})$$

(3)

where, based on the assumption that the universal binding energy relation of Rose et al. [16] contains all the relevant information concerning a single-component system,

$$F^*(a^*) = 1 - (1 + a^*)e^{-a^*},$$

(4)

and where $E_C^{(i)}$ is the cohesive energy of a pure crystal of species i. The scaled lattice parameter a_i^{S*} is given by

$$a_i^{S*} = q\frac{(a_i^S - a_e^i)}{l_i}$$

(5)

where a_i^S is the lattice parameter of the equivalent crystal associated with the defect, a_e^i and l_i are the equilibrium lattice parameter and scaling length [16] of a pure crystal of species i respectively, and $q^3 = 3/16\pi$ for fcc crystals. Although ε_i^S can be obtained via ECT [6], it does not have to be necessarily so, and a_i^{S*} can be obtained as a *solution* of eq.(3) if ε_i^S is computed by any other technique. Either way, a_i^{S*} can be readily obtained, with which we define the coupling term g_i as

$$g_i = e^{-a_i^{S*}}$$

(6)

As in previous efforts, we choose ECT [6] to perform strain energy calculations, the choice being guided by the simplicity and reliability of this technique. Using ECT for computing ε_i^S introduces the added advantage that a_i^S (and thus a_i^{S*}) is directly obtained by solving the

6

ECT equation for the defect crystal, as shown below. Within the framework of ECT, a_i^S is interpreted as the lattice parameter of an ideal, perfect crystal (i.e., the equivalent crystal) where the energy per atom is the same as the energy of atom i in the actual, defect crystal.

In general, the ECT equation for computing the strain energy reads

$$NR_1^p e^{-\alpha R_1} + MR_2^p e^{-(\alpha+\frac{1}{\lambda})R_2} = \sum_j r_j^p e^{-(\alpha+S(r_j))r_j} \tag{7}$$

(see ref. [6] for details) where the quantities p, α, λ and the screening function $S(r)$ are defined in ref. [6]. The sum on the r.h.s. of Eq. (7) runs over all neighbors of atom i at a distance r_j. Eq. (7) is then solved for the lattice parameter of the equivalent crystal a_i^S. R_1 and R_2 are the corresponding nearest- and next-nearest-neighbor distances in the equivalent crystal. The strain energy is then computed with Eq.(3).

Rigorously, the computation of the strain energy includes four terms (see ref. [6]). In this work, we neglect the three- and four-body terms dealing with the bond angle and face-diagonal anisotropies and retain only the two-body term that accounts for bond-length anisotropies, which we expect to be relevant for atoms in the top (surface) layers. The higher order terms would be proportional to the small local fluctuations of the atomic positions around the equilibrium lattice sites. We expect that the leading term, Eq. (3), will properly account for these small distortions.

The chemical contribution ε_i^C is obtained by an ECT-like calculation. As opposed to the strain energy term, the surrounding atoms *retain their chemical identity*, but are forced to be in equilibrium lattice sites. If N_{ik} (M_{ik}) denotes the number of nearest(next)-neighbors of species k of the atom in question (of species i) then the ECT equation to be solved for the equivalent lattice parameter a_i^C is

$$NR_1^{p_i} e^{-\alpha_i R_1} + MR_2^{p_i} e^{-(\alpha_i+\frac{1}{\lambda_i})R_2} = \sum_k N_{ik} r_1^{p_i} e^{-\alpha_{ik} r_1} + \sum_k M_{ik} r_2^{p_i} e^{-(\alpha_{ik}+\frac{1}{\lambda_i})r_2} \tag{8}$$

where $N(M)$ is the number of nearest(next)-neighbors in the equivalent crystal of species i and $R_1(R_2)$ is the nearest(next)-neighbor distance in the equivalent crystal of lattice parameter a_i^C. r_1 and r_2, are the equilibrium nearest- and next-nearest-neighbor distances in an equilibrium crystal of species i, respectively. The chemical energy is then computed with

$$\varepsilon_i^C = \gamma E_C^i F^*(a_i^{C*}) \tag{9}$$

and

$$\varepsilon_{0_i}^C = \gamma_0 E_C^i F^*(a_{0_i}^{C*}) \tag{10}$$

where $\gamma(\gamma_0) = +1$ if $a_i^{C*}(a_{0_i}^{C*}) \geq 0$ and $\gamma(\gamma_0) = -1$ otherwise, and $a_i^{C*} = q(a_i^C - a_e^i)/l_i$ $(a_i^{C_0*} = q(a_i^{C_0} - a_e^i)/l_i)$. The scaled lattice parameter a_i^{C*} is obtained from Eq.(8) with the parameters α_{ik} listed in ref. [17], and $a_i^{C_0*}$ is computed by solving Eq.(8) but with $\alpha_{ik} = \alpha_i$.

C. The BFS parameters Δ

Using eq.(8) for the calculation of the chemical energy might suggest that this is a rigorous ECT calculation. It is not. In interpreting the change of composition as a 'defect', we are just adapting the basic concept underlying equivalent crystal theory to this case. In the single-crystal ECT, where all the atoms are of the same atomic species, we apply perturbation theory in order to find the energy of the defect crystal. The perturbation is basically due to the difference in potentials between the defect solid and the ground-state crystal. As described in the original formulation of the method [6], it is reasonable to parameterize the first-order contributions to the perturbation expansion as

$$\Delta E \propto R^p e^{-\alpha R} \tag{11}$$

where $p = 2n - 2$ (where n is the atom principal quantum number) and α is a parameter that will primarily reflect the structure of the electron density in the overlap region. In single-crystal ECT the parameter α is determined for metals so that the energy to form a rigid (unrelaxed) vacancy is equal to the experimental value.

To a good approximation, these concepts should remain valid in the case of alloys, and by using eq.(8) we are adopting the same functional form used in ECT to describe the perturbation due to dissimilar atomic species. In order to deal with arbitrary defects and structures in future applications, as well as with multicomponent systems, it is convenient

8

to 'localize' this effect and assume that the global property parameterized by α (i.e., the tails of the overlapping electron densities) can be separated into pairs of interacting atoms. In this approximation, the electron density in the region between two atoms of the same species would not be affected by the presence of neighboring atoms of different species. The perturbation would then be localized in the region between two dissimilar atoms. This assumption justifies the definition of the parameter α_{ik} as

$$\alpha_{ik} = \alpha_i + \Delta_{ki} \tag{12}$$

where α_i is the usual value of α for the pure element i and Δ_{ki} is a correction introduced by the presence of a neighbor of species k. Obviously, $\Delta_{ki} = 0$ if $i = k$. The 'perturbation' parameters Δ_{ki} and Δ_{ik} are the only new parameters introduced in BFS: all other parameters are those corresponding to the pure components of the alloy. Generally, these two parameters are determined by requiring BFS to reproduce the experimental values of the heat of solution in the dilute limit, E^{BA} (the heat of solution of an impurity B in a host A), given by

$$E^{BA} = \frac{d\Delta H}{dx}\bigg|_{x\to 0} \tag{13}$$

where ΔH is the heat of formation of the compound $A_{1-x}B_x$, x being the concentration of B atoms. These parameters have been computed for a variety of fcc and bcc metallic alloys (see ref. [17] for a discussion) and work is under way for hcp-based structures. For completeness, we include both the ECT and BFS parameters for some fcc and bcc elements. Table 1 lists the ECT parameters p, l, α, λ, the cohesive energy E_C and the lattice parameter, while Table 2 displays the values of the BFS parameters Δ_{AB} and Δ_{BA} for some of the alloys of these elements, as well as the experimental values of the heat of solution (eq.(13) in the dilute limit used for fitting the BFS parameters. For the case of Al-Ni, we used the theoretical values computed by Sanchez and Carlsson [18].

III. SURFACE ENERGIES OF ORDERED STRUCTURES

A. Ordered structures of fcc-based binary alloys

In this section we will apply the BFS formalism to the simple problem of computing the surface energy of rigid ordered alloy structures. By rigid we mean that, for the sake of simplicity, we will not allow for individual or collective atomic displacements due to the presence of the surface. However, later on we will show results involving relaxations and compare them with available experimental data.

Several alloys form simple ordered structures for low temperatures [19]. Obviously, the higher the symmetry in the patterns that characterize a given structure, the simpler the calculation is. Fortunately, many alloys are found to have, for specific concentrations, some of the simplest possible structures. Therefore, we will concentrate on these structures, shown in fig. 4, for three concentrations: the $L1_2$ A_3B or AB_3 structures and the $L1_0$ and $L1_1$ structures at 50 % concentration, both being fcc-based. Within the cluster expansion method [21] these structures, together with the pure fcc A and B crystals, form a set of fundamental structures for fcc alloys as these represent the possible structures that can be formed assuming nearest-neighbors interactions only, where a tetrahedral cluster is the unit cell [22]. Therefore, the clusters A_mB_{4-m} ($m = 1, ..., 4$) are the building blocks of the corresponding fcc alloy structures A_1, $L1_2$ and $L1_0$.

B. A simple example

We will consider a simple example: the calculation of the surface energy of a given termination of a $L1_2$ structure of an fcc binary alloy. There are two possible terminations for the (100) $L1_2$ structure of a certain A_3B alloy: a mixed-composition (1:1 A:B) plane alternating with a pure A (1:0 A:B) plane, giving an overall stoichiometry (3:1 A:B), and a pure A plane alternating with mixed-composition planes. These two possible bulk truncations are also possible for the (110) surface, whereas the (111) truncation is always stoichiometric (3:1

A:B). We will concentrate on the (1:1 A:B) Ll$_2$ (100) surface and label the planes parallel to the surface with the index $j = 1, ..., b$ where $j = 1$ corresponds to the surface plane and b labels a certain bulk plane, below which no surface effects are to be considered. By forcing the semi-infinite slab to be rigid and limiting BFS to deal with second-neighbor interactions, the calculation is greatly simplified, as only two planes ($j = 1, 2$) contribute to the surface energy. Because of the high symmetry of this structure, only one atom of each species needs to be considered for the $j = 1$ plane, whereas only one A atom contributes from the plane $j = 2$. Atoms in layers $j = 3, ..., b$ are inert, in that they will not contribute to the surface energy. We will assume that the lattice parameter a is the one previously determined for a bulk ordered alloy A_3B. Let X_j ($X = A, B$; $j = 1, 2$) denote a non-equivalent atom of species X in layer j. We need to compute the contributions σ_{X_j} from A_1, B_1 and A_2 so that the surface energy will be

$$\sigma = \sigma_{A_1} + \sigma_{B_1} + 2\sigma_{A_2} \tag{14}$$

where

$$\sigma_{X_j} = \varepsilon_{X_j}^S + g_{X_j}(\varepsilon_{X_j}^C - \varepsilon_{X_j}^{C_0}) \tag{15}$$

Using eq.(7), the strain energy contribution is computed from the solution of the following equations:

$$12R_1^{p_A} e^{-\alpha_A R_1} + 6R_2^{p_A} e^{-(\alpha_A + \frac{1}{\lambda_A})R_2} = 8r_1^{p_A} e^{-\alpha_A r_1} + 5r_2^{p_A} e^{-(\alpha_A + \frac{1}{\lambda_A})r_2} \quad (X_j = A_1) \tag{16}$$

$$12R_1^{p_B} e^{-\alpha_B R_1} + 6R_2^{p_B} e^{-(\alpha_B + \frac{1}{\lambda_B})R_2} = 8r_1^{p_B} e^{-\alpha_B r_1} + 5r_2^{p_B} e^{-(\alpha_B + \frac{1}{\lambda_B})r_2} \quad (X_j = B_1) \tag{17}$$

and

$$12R_1^{p_A} e^{-\alpha_A R_1} + 6R_2^{p_A} e^{-(\alpha_A + \frac{1}{\lambda_A})R_2} = 12r_1^{p_A} e^{-\alpha_A r_1} + 5r_2^{p_A} e^{-(\alpha_A + \frac{1}{\lambda_A})r_2} \quad (X_j = A_2), \tag{18}$$

where $r_1 = \sqrt{2}a/2$ and $r_2 = a$. The equivalent lattice parameters $a_{X_j}^S$ are obtained from the solutions to eqs.(16)-(18) as $a_{X_j}^S = \sqrt{2}R_1(j) = R_2(j)$ and the strain energy contributions $\varepsilon_{X_j}^S$ are computed using eq(4).

Using eq.(8), the chemical energy contribution $\varepsilon_{X_j}^C$ is computed from the solution of the following equations:

$$12R_1^{pA}e^{-\alpha_A R_1} + 6R_2^{pA}e^{-(\alpha_A + \frac{1}{\lambda_A})R_2} = 4d_1^{pA}e^{-\alpha_A d_1} + 4d_1^{pA}e^{-(\alpha_A + \Delta_{BA})d_1} + 5d_2^{pA}e^{-(\alpha_A + \frac{1}{\lambda_A})d_2}$$

$$(X_j = A_1) \qquad (19)$$

$$12R_1^{pB}e^{-\alpha_B R_1} + 6R_2^{pB}e^{-(\alpha_B + \frac{1}{\lambda_B})R_2} = 4s_1^{pB}e^{-\alpha_B s_1} + 4s_1^{pB}e^{-(\alpha_B + \Delta_{AB})s_1} + 5s_2^{pB}e^{-(\alpha_B + \frac{1}{\lambda_B})s_2}$$

$$(X_j = B_1) \qquad (20)$$

and

$$12R_1^{pA}e^{-\alpha_A R_1} + 6R_2^{pA}e^{-(\alpha_A + \frac{1}{\lambda_A})R_2} = 8d_1^{pA}e^{-\alpha_A r_1} + 4d_1^{pA}e^{-(\alpha_A + \Delta_{BA})d_1} + 5r_2^{pA}e^{-(\alpha_A + \frac{1}{\lambda_A})r_2}$$

$$(X_j = A_2), \qquad (21)$$

where $d_1 = \sqrt{2}a_e^A/2$, $r_2 = a_e^A$, $s_1 = \sqrt{2}a_e^B/2$ and $s_2 = a_e^B$. The equivalent lattice parameters $a_{X_j}^C$ are obtained from the solutions to eqs.(19)-(21) as $a_{X_j}^C = \sqrt{2}R_1(j) = R_2(j)$. Remembering that $\gamma_{X_j} = \pm 1$ whether $a_{X_j}^{C*} = q(a_{X_j}^C - a_e^X)/l_X$ is positive or negative, the first term in the chemical contribution, $\varepsilon_{X_j}^C$ is then

$$\varepsilon_{X_j}^C = \gamma_{X_j} E_C^{(X)} F^*(a_{X_j}^{C*}) \qquad (22)$$

Finally, the reference to the chemical energy, $\varepsilon_{X_j}^{C_0}$ is computed from the solution of the following equations:

$$12R_1^{pA}e^{-\alpha_A R_1} + 6R_2^{pA}e^{-(\alpha_A + \frac{1}{\lambda_A})R_2} = 8d_1^{pA}e^{-\alpha_A d_1} + 5d_2^{pA}e^{-(\alpha_A + \frac{1}{\lambda_A})d_2} \quad (X_j = A_1) \qquad (23)$$

$$12R_1^{pB}e^{-\alpha_B R_1} + 6R_2^{pB}e^{-(\alpha_B + \frac{1}{\lambda_B})R_2} = 8s_1^{pB}e^{-\alpha_B s_1} + 5s_2^{pB}e^{-(\alpha_B + \frac{1}{\lambda_B})s_2} \quad (X_j = B_1) \qquad (24)$$

and

$$12R_1^{pA}e^{-\alpha_A R_1} + 6R_2^{pA}e^{-(\alpha_A + \frac{1}{\lambda_A})R_2} = 12d_1^{pA}e^{-\alpha_A d_1} + 5d_2^{pA}e^{-(\alpha_A + \frac{1}{\lambda_A})d_2} \quad (X_j = A_2), \qquad (25)$$

The equivalent lattice parameters $a_{X_j}^{C_0}$ are obtained from the solutions to eqs.(23)-(25) as $a_{X_j}^{C_0} = \sqrt{2}R_1(j) = R_2(j)$ and the reference chemical energy contributions $\varepsilon_{X_j}^{C_0}$ are computed using eq(10).

IV. APPLICATION TO SURFACE STRUCTURE

The determination of the surface structure of alloys has recently been the topic of theoretical and experimental work. Much effort has been devoted to the study of surface relaxation in metals and, to a lesser extent, alloys. Several recent experiments have provided insights in the phenomena of surface relaxation and composition, in the case of alloys, and correspondingly a number of theoretical studies have shown good general agreement with experimental results.

However, there is still a great deal of uncertainty in certain areas, due to limitations inherent in experimental techniques and also to the lack of alternative studies to verify previous results.

The first experiment, in 1984, that provided detailed information on the atomic positions of surface atoms in a truncated ordered alloy is the low-energy electron diffraction (LEED) intensity analysis of Davis and Noonan of a NiAl(110) surface [2]. They found strong evidence for a rippled surface, where the Al sites of the top layer (in the mixed-composition truncation) are displaced above the Ni sites by approximately 0.22 Å. This result was quickly followed by the calculation performed by Chen, Voter and Srolovitz using the embedded atom method (EAM) [23], which confirmed the main features found in the experiment. EAM was later used to investigate similar phenomena in other ordered alloys: Foiles and Daw presented a complete study of Ni_3Al ($L1_2$ structure) [24], followed by Foiles work on ordered surface phases of Au on Cu [25], and Lundberg's extensive study of surface segregation and relaxation of Pt-Ni alloys [26]. At the same time, new experimental LEED results on Ni_3Al were reported by Sondericker and coworkers [3], finding a similar rippled structure in Ni_3Al (100) faces. Finally, a low-energy ion scattering spectroscopy (LEISS) experiment by Wang and coworkers provided similar data for the Cu_3Au system, a classic ordering alloy [4]. Their work followed the LEISS results concerning the surface composition of the top atomic layers [27]. This system was also the subject of a very recent study by Wallace and Ackland using a molecular statics algorithm with Finnis-Sinclair (FS) many-body potentials [28].

13

In this section we will show new results concerning the above mentioned systems as well as predictions for other alloys, using BFS. Due to its computational efficiency, this application of BFS to the surface structure of ordered alloys extends to a number of systems for which there are no other theoretical or experimental studies to date.

Before proceeding to the calculation of multilayer relaxation in alloys, we will discuss some features of theoretical calculations of these quantities. Ref. [1] provides a reasonably large sample of both experimental and theoretical results for changes in interlayer spacing in pure crystals. In all cases, the theoretical techniques used rely either on the use of input data (generally experimentally determined) or on certain approximations for some of the variables of relevance. Necessarily, the results will depend on such choices. Multilayer relaxations involve at best very small changes in position, and correspondingly, comparable changes in surface energy, whose minimization is the criterion used to determine the final interlayer spacings. Thus, the search for a minimum of the surface energy, as accurate as the minimization technique might be, will be strongly influenced by the two factors indicated above: the approximations used and the shallowness of the minimum in the surface energy surface resulting from small changes in the input parameters. As a consequence, to quote just one value for each of the changes in interlayer spacings as is ordinarily done, might not reflect the ambiguities in these calculations. In this paper we adopt a different path: to each theoretical prediction, we will attach an estimate of the possible errors due to any of the reasons mentioned above. Although there is no certain way to determine such errors (after all, the predictions are, within their own framework, exact), we will see that changes on the order of 1 % in the surface energy can generate quite interesting variations in the relaxation schemes predicted. In particular, within the framework of ECT, such small changes in the surface energy can be easily obtained by changing any of the input parameters (lattice constant, cohesive energy, bulk modulus) by a similar amount, well below the usual experimental errors in the determination of such quantities.

To illustrate this issue, we will focus our attention on the surface structure of some fcc pure metals (Al, Au, Cu and Ni). As can be seen in Tables 2-11 of ref. [1], previous

theoretical and experimental studies show a wide spread in the predictions of the changes in interlayer spacings for the (100) and (110) surfaces. Even results obtained within the same theoretical technique (EAM, ECT) do not agree with each other (due to different fitting procedures of the embedding function in the case of EAM and different input data in both cases). Although there is general qualitative agreement, regarding the contraction or expansion pattern found for successive layers, in some cases the theoretical values show poor agreement with experimental results (see, for example, Al (100)). The ECT results (from refs. [1] and [6]) also highlight this inconsistency. The difference between the values obtained in this work and those from previous applications of ECT is easily traceable to slightly different values of some of the input parameters.

As mentioned above, in order to account for these and other ambiguities in the calculation, we investigated the change in predicted relaxations due to small changes in the rigid surface energy. We thus defined 'error bars' in such way that all the intermediate values so obtained predict variations in surface energies within that tolerance. Needless to say, this range of values does not include all the possible sets (Δd_{12}, Δd_{23}) that correspond to surface energies within the allowed values. It is interesting to note, however, that in most cases, all the experimental as well as theoretical predictions fall within the range of values obtained in this fashion.

It should be noted that when comparing our theoretical predictions with available experimental results, the error bars quoted in each case are not rigourously comparable. However, we choose to do so with the only purpose of giving a complete description of the results obtainable with ECT and BFS, once uncertainties in the input parameters are taken into account. To illustrate this point, we first discuss the surface energies and multilayer relaxations of the unreconstructed low-index surfaces of pure Al, Ni, Cu and Au crystals. In Table 1 we display the ECT predictions for the surface energies and compare the results with typical experimental values for polycrystalline samples [29–31]. The agreement is excellent in all cases, with the exception of Cu, that shows a somewhat larger deviation than the other elements. We note that experimental values for the surface energies are for polycrystalline

15

surfaces, thus could be strongly dominated by the predominant surface plane.

In table 2 we compare results for the multilayer relaxations of the first two interlayer spacings for those cases for which recent experimental data is available [32–41]. Once again the agreement is excellent, as it was shown in previous ECT studies of surface structure [1]. The inclusion of the theoretical 'error bar', as mentioned above, allows for a better comparison with experiment as it shows that for most cases, small changes in the input parameters of the method suffice to account for the whole range of possible experimental results. The exceptions are Al(100) and Al(111), where the outward relaxation of the surface layer has been attributed to an electron promotion effect [41]. Semiempirical methods (ECT, EAM. etc.), unless specifically designed to do so, do not generally allow for such fine electronic structure effects, thus it is not surprising that our results for Δd_{12} in these cases predict surface layer contractions, even when the 'error bar' is taken into account. For completeness we also include results for the surface relaxation when only that plane is allowed to relax, in order to single out the influence of subsequent interlayer spacing changes on the surface plane. Again, the agreement with available experimental data is very good in all cases.

As mentioned above, there are few theoretical or experimental studies of ordered alloy surfaces [2–4,23–28]. First, we discuss two cases (Ni_3Al and Cu_3Au, in the $L1_2$ structure) which have been the subject of recent studies [3,4,23,24]. We follow this discussion with a complete presentation of the corresponding results for a larger number of ordered structures as well as different binary alloys of fcc elements, for which no theoretical or experimental data exists.

a. Cu_3Au: Table 5 displays the results for the unrelaxed and relaxed surface energies (in ergs/cm^2) as obtained with BFS and with FS many-body potentials [28]. Both methods predict, as expected, lower surface energies for the mixed-composition (100) and (110) truncations. This feature has been experimentally proven via a low-energy ion scattering study which detected equal parts of Cu and Au in the top layer [27]. ECT and FS results also agree on the relative change in surface energy once the top-most layers are allowed to relax, in spite of the fact that the FS values are 50 % smaller than the BFS ones. As is

also to be expected, the surface energies of (100)1:0 and (110)1:0 faces are comparable to the corresponding values for single Cu crystals. The corresponding relaxations are quoted in table 4. In order to avoid ambiguities in determining the exact atomic positions from the entries in table 4, we present the relaxations as the percentage change in interlayer spacing from the unrelaxed case to the one measured from the relaxed position to the unrelaxed location of the plane immediately below. We also include the BFS predictions for the pure Cu truncations of the (100) and (110) planes. Although it is to be expected that the top layer relaxation will change as deeper layers are allowed to relax, any ensuing changes would be small, not affecting the conclusions drawn from our results.

For the Cu_3Au (100) 1:1 Cu:Au case, the results in table 6 imply a rippling of 0.148 ± 0.025 Å, which amounts to 3.97 % of the lattice parameter determined for this alloy (3.73 Å). This result compares very well with the 3.77 % rippling (Al out, Ni in) obtained using FS potentials. A similar situation is found for the (110) 1:1 Cu:Au surface, where we find the rippling to be 4.2 ± 1.1 % of the lattice parameter, whereas FS potentials predict a rather smaller change of 1.9 %. For the mixed-composition (111) 3:1 Cu:Au surface, BFS predicts a rippling of 4.6 ± 0.4 % thus agreeing with FS results and experimental evidence that the Au atoms are farther out than the neighboring Cu atoms in mixed-composition surfaces.

b. *Ni_3Al.* The surface energies of relaxed (100), (110) and (111) surfaces are shown in Table 7, where we compare our results with the EAM study of Foiles and Daw [24]. As found for the Cu_3Au case, the mixed-composition truncations always have a lower surface energy. The differences between the EAM and BFS predictions are consistent with previous calculations for pure metals, where the EAM results are typically 50 % lower than the experimental ones. Surface relaxations are indicated in Table 8, using the same format and notation of table 4. From these results we extract the following values for the gap between Ni and Al atoms in the mixed-composition (100), (110) and (111) surfaces: 0.12 ± 0.04 Å, 0.09 ± 0.05 Å and 0.16 ± 0.03 Å, respectively. A similar trend, but with somewhat smaller values for the rippling are obtained from EAM [23]: 0.09 Å, 0.06 Å and 0.07 Å. A different EAM calculation [25] predicts a 0.06 Åseparation between Ni and Al atoms in all three

17

surfaces. Recent LEED data [3] show $\Delta d_{12}(Ni) = -2.73\%$ and $\Delta d_{12}(Al) \sim 0$ (i.e., Al is displaced outward with respect to Ni) and a rippling of 0.02±0.03 Åfor the (100) surface

c.*Other fcc binary alloys* Table 9-11 display results similar to the ones described previously for Ni-Al and Cu-Au alloys, indicating, when appropriate, the distance between the atoms of different species in the top layer of each surface. Table 9 includes the results for the three possible terminations of the L1$_0$ structure (1:1, 0:1 and 1:0) whereas Table 10 shows the results for the (100)1:1 surface of the L1$_1$ ordered structure. Finally, Table 11 shows an extensive set of results of A_3B and AB_3 alloys in the L1$_2$ structure, as shown in fig. 4.

In general, surface energies vary widely for each system, depending on the type of structure and crystal face considered. There is no apparent pattern that describes trends among all the different systems discussed in this work. For example, although there is some correlation between the lattice mismatch and the ripple between the surface atoms in the mixed termination surfaces of the L1$_0$ alloys, in that the vertical separation between atoms of different species on the surface increases with the lattice mismatch, there is also an exceptional case, like Cu-Pd, with a very large rippling effect. The ordering of the surface energies varies from alloy to alloy covering a wide range of values. With very few exceptions, the planar relaxations are small, with even smaller uncertainty factors which in turn translates into small uncertainties in the rippling of the mixed-termination surfaces.

Obviously, not all the listed structures exist in nature. We are presenting this survey with the only purpose of highlighting the simplicity of alloy surface energy calculation with BFS and the predictive power of the method. In this sense, the results presented in this work will hopefully motivate the development of new experiments in the determination of surface structure.

V. CONCLUSIONS

In this paper we presented an extended discussion on BFS, a semiempirical method for alloys, concentrating in aspects of surface structure. The application of BFS to the calculation of the surface energy of an ordered alloy highlights the computational simplicity of this method, which is an essential ingredient of any algorithm used for the determination and simulation of materials properties. The results on multilayer relaxation of ordered structures, and their comparison with available experimental values, provide a good example of the quality of the results that can be obtained with this method. This, together with the numerical efficiency of this technique, makes BFS an appropriate tool for dealing with more complex situations, like those found in realistic problems in alloy structure.

ACKNOWLEDGMENTS

REFERENCES

[1] A. M. Rodríguez, G. Bozzolo and J. Ferrante, Surf. Sci. **289**, 100 (1993) and refrences therein.

[2] H. L. Davis and J. R. Noonan, Phys. Rev. Lett. **54**, 566 (1985).

[3] D. Sondericker, F. Jona and P. M. Marcus, Phys. Rev. B **33**, 900 (1986).

[4] Q. Whang, Y. S. Li, C. K. C. Lok, J. Quinn, F. Jona and P. M. Marcus, Sol. State Comm. **62**, 181 (1987).

[5] G. Bozzolo and J. Ferrante and J. R. Smith, Phys. Rev. B **45**, 493 (1992).

[6] J. R. Smith, T. Perry, A. Banerjea, J. Ferrante and G. Bozzolo, Phys. Rev. B **44**, 6444 (1991).

[7] G. Bozzolo and J. Ferrante, Phys. Rev. B **45**, 12191 (1992).

[8] G. Bozzolo and J. Ferrante, Scripta Met. Mater. **26**, 1275 (1992).

[9] G. Bozzolo and J. Ferrante, Ultramicroscopy **42/44**, 55 (1992).

[10] B. Good, G. Bozzolo and J. Ferrante, Phys. Rev. B **48**, 18284 (1993).

[11] R. Kobistek, G. Bozzolo, J. Ferrante and H. Schlosser, Surf. Sci. **307/309**, 390 (1994).

[12] G. Bozzolo and J. Ferrante, Mat. Res. Soc. Symp. Proc. **291**, 389 (1993).

[13] G. Bozzolo, B. Good and J. Ferrante, Surf. Sci. **289**, 169 (1993).

[14] G. Bozzolo and J. Ferrante, Phys. Rev. B (in press).

[15] L. Vegard, Z. Physik **5**, 17 (1921).

[16] J. H. Rose, J. R. Smith and J. Ferrante, Phys. Rev. B **28**, 1835 (1983); J. H. Rose, J. R. Smith, F. Guinea and J. Ferrante, Phys. Rev. B **29**, 2963 (1984).

[17] G. Bozzolo and J. Ferrante, Phys. Rev. B **46** , 8600 (1992).

[18] A. E. Carlsson and J. M. Sanchez, Solid State Commun. **65**, 527 (1988).

[19] R. Hultgren, R. L. Orr, P. D. Anderson and K. K. Kelley, *Selected Values of the Thermodynamic Properties of Binary Alloys* (Wiley, New York, 1963).

[20] T. Mohri, J. M. Sanchez and D. de Fontaine, Acta Metall. **33**, 1171 (1985).

[21] R. Kikuchi, Phys. Rev. **81**, 988 (1951); J. Chem. Phys. **60**, 1071 (1974).

[22] J. W. D. Connolly and A. R. Williams, Phys. Rev. B **27**, 5169 (1983).

[23] S. P. Chen, A. F. Voter and D. J. Srolovitz, Phys. Rev. Lett. **52**, 1308 (1986).

[24] S. M. Foiles and M. S. Daw, J. Mater. Res. **2**, 5 (1987).

[25] S. M. Foiles, Surf. Sci. **191**, 329 (1987).

[26] M. Lundberg, Phys. Rev. B **36**, 4692 (1987).

[27] T. M. Buck, G. H. Wheatley and L. Marchut, Phys. Rev. Lett. **51**, 43 (1983).

[28] W. E. Wallace and G. J. Ackland, Surf. Sci. Lett. **275**, L685 (1992).

[29] W. R. Tyson, J. Appl. Phys. **47**, 459 (1976).

[30] W. R. Tyson and W. A. Miller, Surf. Sci. **62**, 267 (1977).

[31] H. Wawra, Z. Metallk. **66**, 395 (1975).

[32] H. L. Davis, J. B. Hannon, K. B. Ray and E. W. Plummer, Phys. Rev. Lett. **68**, 2632 (1992).

[33] J. R. Noonan and H. L. Davis, Phys. Rev. B **29**, 4349 (1984).

[34] J. R. Noonan and H. L. Davis, J. Vac. Sci. Technol. A8, 2671 (1990).

[35] J. W. M. Frenken, J. F. van der Veen and G. Allan, Phys. Rev. Lett. **51**, 1876 (1983).

[36] S. M. Yalisove, W. R. Graham, E. D. Adams, M. Copel and T. Gustafsson, Surf. Sci.

171, 400 (1986).

[37] J. E. Demuth, P. M. Marcus and D. W. Jepsen, Phys. Rev. **11**, 1460 (1975).

[38] R. Mayer, C. Zhang, K. G. Lynn, W. E. Frieze, F. Jona and P. M. Marcus, Phys. Rev. B **35**, 3102 (1987).

[39] I. Stensgaard, R. Feidenhans'l and J. E. Sorensen, Surf. Sci. **128**, 281 (1983).

[40] S. A. Lindgren, L. Wallden, J. Rundgren and P. Westrin, Phys. Rev. B **29**, 576 (1984).

[41] P. J. Feibelman, Phys. Rev. B**46**, 2532 (1992).

Element	Cohesive Energy	Lattice Constant	p	l	α	λ
Al	3.34	4.05	4	0.336	2.105	0.944
Cu	3.50	3.615	6	0.272	2.935	0.765
Ag	2.96	4.086	8	0.269	3.337	0.756
Au	3.78	4.078	10	0.236	4.339	0.663
Ni	4.435	3.524	6	0.270	3.015	0.759
Ir	6.94	3.84	10	0.235	4.408	0.661
Pd	3.94	3.89	8	0.237	3.612	0.666
Pt	5.85	3.92	10	0.237	4.535	0.666
Fe	4.27	3.57	6	0.279	2.963	0.784
W	8.66	3.16	10	0.274	4.232	0.770
Ta	8.10	3.30	10	0.325	3.905	0.914
Mo	6.82	3.15	8	0.262	3.420	0.736
Nb	7.57	3.30	8	0.341	3.243	0.958
V	5.31	3.03	6	0.305	2.726	0.857
Cr	4.10	2.88	6	0.254	2.889	0.714
Fe	4.29	2.86	6	0.277	3.124	0.770
Li	1.63	3.491	2	0.589	1.049	1.66
Na	1.113	4.225	4	0.578	1.359	1.62
K	0.934	5.225	6	0.694	1.528	1.95
Rb	0.852	5.585	8	0.651	1.937	1.83
Cs	0.804	6.045	10	0.757	2.115	2.13

Table 1: Experimental input: Cohesive energy (in eV), lattice parameter (in Å). ECT parameters: p, l (in Å), α (in Å^{-1}) and λ (in Å) for several fcc elements.

A-B	Δ_{AB}	Δ_{BA}	E^{sol}_{AB}	E^{sol}_{BA}
Ag-Al	0.0475	-0.0499	0.141	-0.166
Ag-Au	-0.0333	-0.0227	-0.161	-0.186
Ag-Cu	-0.0391	-0.0308	0.392	0.250
Ag-Pd	-0.0451	-0.0178	-0.108	-0.288
Al-Au	-0.0501	-0.0853	-1.26	-0.80
Al-Cu	-0.0526	-0.0626	-0.35	-0.20
Al-Ni	-0.0657	-0.0861	-1.715	-0.494
Au-Cu	-0.0513	-0.0604	-0.191	-0.126
Au-Ni	-0.0506	-0.0622	0.280	0.218
Au-Pd	-0.0460	-0.0345	-0.195	-0.356
Cu-Fe	0.0495	0.0638	0.412	0.349
Cu-Ni	-0.0163	0.0309	0.100	0.032
Cu-Pd	-0.0431	-0.0495	-0.392	-0.436
Cu-Pt	-0.0585	-0.0441	-0.299	-0.532
Fe-Ni	-0.0106	-0.0320	-0.218	-0.079
Fe-Pd	-0.0229	-0.0584	-0.656	0.177
Ni-Pd	-0.0396	-0.0478	-0.088	0.057
Ni-Pt	-0.0609	-0.0537	-0.330	-0.282
Cr-Fe	0.0465	0.0285	0.218	0.218
Cr-Mo	-0.02447	-0.0090	-0.102	0.807
Cr-V	-0.0246	-0.0232	-0.088	-0.189
Fe-V	0.0998	-0.07168	0.215	0.323

Table 2: Parameters Δ_{AB} and Δ_{BA} (in Å^{-1}) and heats of solution in the dilute limit E^{sol}_{AB} and E^{sol}_{BA} (in eV/atom) for several fcc binary alloys. The values for Al-Ni were obtained from a theoretical calculation by Sanchez and Carlsson [18] .

25

Technique	Al	Cu	Ni
Exp. [29]	1200	1790	2270
Exp. [30]	1140	1780	2380
Exp. [30]	1180	1770	2240
Exp. [31]	1169	2016	2664
ECT(100)	1203	2309	2982
ECT(110)	1284	2373	3073
ECT(111)	856	1767	2274

Table 3: Surface energies (in ergs/cm^2) of fcc Al, Cu and Ni

Element	Face	Experiment			ECT	ECT	(two-layers)
		Δd_{12}	Δd_{23}	Ref.	Δd_{12}	Δd_{12}	Δd_{23}
Al	(100)	+1.8		[32]	-4.68±1.62	-5.05±1.58	+3.35±0.80
	(110)	-8.5±1.0	+5.5±1.1	[33]	-8.29±2.35	-9.53±3.58	+1.90±2.24
	(111)	+1.7±0.3	+0.5±0.7	[34]	-3.67±1.21	-3.94±1.19	+2.75±0.61
Ni	(100)	-3.2±0.5		[35]	-3.53±1.68	-3.82±1.68	+2.48±0.85
	(110)	-9.0±1.0	+3.5±1.5	[36]	-6.32±2.44	-6.55±3.63	+0.34±2.24
	(111)	-1.2±1.2		[37]	-2.89±1.29	-3.10±1.25	+2.12±0.63
Cu	(100)	-2.1	+0.45	[38]	-3.52±1.74	-3.81±1.70	+2.47±0.86
	(110)	-7.5±1.5	+2.5±1.5	[39]	-6.31±2.46	-6.51±3.83	+0.29±2.44
	(111)	-0.7±0.5		[40]	-2.88±1.30	-3.10±1.25	+2.12±0.63

Table 4: Surface relaxations of Al, Cu and Ni as percentages of the rigid interplanar spacings.

Face	Finnis-Sinclair [28]		BFS	
	Unrelaxed	Relaxed	Unrelaxed	Relaxed
(100)1:1	896	865	2119	1810
(100)1:0	1192	1171	2478	2247
(110)1:1	1051	1024	2397	2337
(110)1:0	1240	1173	2873	2699
(111)3:1	882	863	1626	1577

Table 5: Unrelaxed and relaxed surface energies (in ergs/cm^2) of Cu$_3$Au.

Layer	Atom	(100)1:1	(100)1:0	(110)1:1	(110)1:0	(111)3:1
1	Cu	-2.12±0.41	+5.38±0.47	-2.45±1.14	-3.70±1.02	+14.35±0.26
	Au	+5.82±0.81	-	+7.80±1.80	-	+22.29±0.53
2	Cu	+5.61±0.37	+12.87±0.50	+10.14±1.37	+12.14±1.37	+21.20±0.24
	Au	-	+3.23±1.23	-	-0.70±1.30	+2.23±1.92

Table 6: Surface relaxations of Cu$_3$Au L1$_2$ surfaces. See text for definition of the percentage change.

27

Face	EAM [24]	BFS
(100)1:1	1620	2852
(100)1:0	1885	3168
(110)1:1	1730	3117
(110)1:0	1920	3964
(111)3:1	1645	2411

Table7 : Surface energies of Ni_3Al (in ergs/cm^2).

Layer	Atom	(100)1:1	(100)1:0	(110)1:1	(110)1:0	(111)3:1
1	Ni	-1.33±0.70	+3.41±0.72	-4.63±1.65	-5.03±1.31	+8.56±0.55
	Al	+5.25±1.60	-	+0.80±2.85	-	+16.28±1.40
2	Ni	+4.59±0.63	+8.82±0.81	+3.55±2.19	+5.19±2.40	+13.69±0.53
	Al	-	+3.39±1.46	-	+0.92±2.74	+4.04±1.53

Table 8 : Surface relaxations of Ni_3Al $L1_2$ surfaces. See text for definition of the percentage change.

Al-Ni

Face	σ	Δ^A_{12}	Δ^B_{12}	Δ^A_{23}	Δ^B_{23}	Ripple
(100)1:1	2028.52	+3.92±0.82	-3.18±0.24	+0.94±0.64	+6.56±0.25	0.13165±0.01972
(100)1:0	788.52	-3.73±0.28			+2.59±0.29	
(100)0:1	3987.35		-3.72±0.92	+0.98±0.96		
(110)1:0	2074.33	-2.80±2.02			-10.46±0.67	
(110)0:1	3296.91		-11.14±0.54	-1.54±1.39		

Cu-Au

Face	σ	Δ^A_{12}	Δ^B_{12}	Δ^A_{23}	Δ^B_{23}	Ripple
(100)1:1	1451.49	-1.83±0.18	+6.07±0.50	+8.87±0.18	+1.00±0.46	0.15423±0.01314
(100)1:0	2572.39	-0.75±0.93			+0.18±0.97	
(100)0:1	1344.69		-2.86±0.37	+0.20±0.36		
(110)1:0	1999.26	-11.63±0.42			-2.99±0.61	
(110)0:1	2033.18		-1.66±1.25	-8.79±0.96		

Cu-Pd

Face	σ	Δ^A_{12}	Δ^B_{12}	Δ^A_{23}	Δ^B_{23}	Ripple
(100)1:1	2021.80	-2.18±0.40	-13.01±0.63	-5.02±0.97	+8.28±0.41	0.20400±0.01932
(100)1:0	2504.42	-12.81±0.56			-6.13±0.51	
(100)0:1	1768.69		-4.98±0.31	+2.94±0.32		
(110)1:0	2179.96	-11.35±0.52			-3.20±1.90	
(110)0:1	2384.95		-19.80±1.34	-6.39±1.85		

Cu-Pt

Face	σ	Δ^A_{12}	Δ^B_{12}	Δ^A_{23}	Δ^B_{23}	Ripple
(100)1:1	2146.96	-2.74±0.29	+3.27±0.46	+6.86±0.28	+0.61±0.47	0.11482±0.0143
(100)1:0	2585.38	-0.69±0.82			+0.34±0.85	
(100)0:1	2323.20		-2.66±0.42	+0.32±0.41		
(110)1:0	2388.02	-10.07±0.66			-2.47±0.71	
(110)0:1	2935.28		-1.99±0.92	+2.37±1.62		

Ag-Au

Face	σ	Δ^A_{12}	Δ^B_{12}	Δ^A_{23}	Δ^B_{23}	Ripple
(100)1:1	1543.26	-5.69±0.55	-3.81±0.36	+0.79±0.48	-1.78±0.46	0.03856±0.01856
(100)1:0	1598.66	-3.62±0.44			-0.22±0.48	
(100)0:1	1561.59		-6.34±0.38	-2.61±0.35		
(110)1:0	1600.28	-9.96±1.10			-3.13±1.12	
(110)0:1	1675.03		-5.44±0.55	-0.33±1.35		

Table 9 : Surface energies (in ergs/cm^2), planar relaxations (as percentages of the rigid interplanar spacing, see text) of the top two layers of several low-index faces of the L1$_0$ ordered structure. Δ^X_{ij} indicates the relaxation between layers i and j for an atom of species X in layer i. The last column indicates the difference (in Å) between the position of an atom A and an atom B in the top layer.

Au-Pd

Face	σ	Δ^A_{12}	Δ^B_{12}	Δ^A_{23}	Δ^B_{23}	Ripple
(100)1:1	1953.39	-0.37±0.57	-4.06±0.60	-0.25±0.50	+2.76±0.71	0.07415±0.02355
(100)1:0	1404.01	-2.84±0.44			-0.09±0.41	
(100)0:1	2668.31		-1.42±0.80	+0.32±0.79		
(110)1:0	1976.47	-2.96±0.95			+0.39±1.63	
(110)0:1	2364.57		-7.79±1.24	-1.38±1.11		

Ni-Pd

Face	σ	Δ^A_{12}	Δ^B_{12}	Δ^A_{23}	Δ^B_{23}	Ripple
(100)1:1	1717.93	-8.55±0.26	-13.06±0.68	-7.92±0.30	+2.44±0.28	0.08520±0.01768
(100)1:0	2176.18	-15.98±0.29			-7.94±0.23	
(100)0:1	1255.65		-9.01±0.19	-0.71±0.21		
(110)1:0	1980.87	-12.61±0.31			-5.14±1.51	
(110)0:1	1902.53		-19.89±1.16	-10.47±0.49		

Ni-Pt

Face	σ	Δ^A_{12}	Δ^B_{12}	Δ^A_{23}	Δ^B_{23}	Ripple
(100)1:1	2153.11	-4.63±0.18	+2.08±0.44	+5.87±0.19	-0.87±0.41	0.12808±0.01181
(100)1:0	3248.61	-3.75±0.68			-1.60±0.73	
(100)0:1	2228.15		-5.60±0.35	-1.94±0.33		
(110)1:0	2519.11	-11.94±0.39			-3.38±0.61	
(110)0:1	3057.54		-2.66±1.13	-9.56±0.83		

Table 9: (Cont'd)

Alloy	σ	Δ^A_{12}	Δ^B_{12}	Δ^A_{23}	Δ^B_{23}	Ripple
Al-Ni	1442.33	+1.97±0.67	-5.14±0.16	-0.89±0.54	+5.18±0.17	0.13379±0.01566
Cu-Au	1205.58	-2.61±0.15	+5.25±0.44	+8.26±0.15	+0.44±0.41	0.15463±0.01155
Cu-Pd	1816.93	-2.30±0.39	-13.64±0.67	-6.08±0.75	+8.38±0.41	0.21487±0.02022
Cu-Pt	1964.02	-3.31±0.24	+2.81±0.44	+6.59±0.24	+0.25±0.45	0.11756±0.07319
Ag-Au	1526.48	-5.91±0.54	-4.00±0.35	+0.69±0.47	-1.96±0.46	0.03921±0.01829
Au-Pd	1885.63	-0.47±0.55	-4.40±0.58	-0.41±0.49	+2.89±0.68	0.07898±0.02290
Ni-Pd	1549.94	-8.06±0.23	-13.20±0.62	-8.03±0.27	+3.04±0.25	0.09749±0.01626
Ni-Pt	1856.99	-5.02±0.16	+1.64±0.39	-5.61±0.16	-1.18±0.38	0.12788±0.01051

Table 1Q: Surface energies σ (in ergs/cm^2), planar relaxations (as percentages of the rigid interplanar spacing, see text) of the top two layers of the (100)1:1 surface of the L1$_1$ ordered structure. Δ^X_{ij} represents the relaxation between planes i and j for an atom of species X in layer i. The last column indicates the difference in position (in Å) between an atom A and an atom B in the top layer.

31

Cu$_3$Au

Face	σ	Δ^A_{12}	Δ^B_{12}	Δ^A_{23}	Δ^B_{23}	Ripple
(100)1:1	1922.98	-6.51±0.30	+1.42±0.66	+1.67±0.28		0.14941±0.01823
(100)1:0	2205.44	+2.36±0.33		+10.47±0.35	+1.33±0.85	
(110)1:1	2453.12	-3.63±0.85	+6.58±1.48	+10.00±0.85		
(110)1:0	2649.79	-8.07±0.61		+7.56±1.17	-2.65±0.86	
(111)3:1	1309.49	+8.60±0.22	+16.68±0.52	+15.93±0.20	+2.48±0.87	0.17583±0.01601

Au$_3$Cu

Face	σ	Δ^A_{12}	Δ^B_{12}	Δ^A_{23}	Δ^B_{23}	Ripple
(100)1:1	2050.03	+1.47±0.83	-3.89±0.41	+1.18±0.37		0.10733±0.02479
(100)1:0	1285.48	-0.12±0.26		+0.91±0.48	+5.03±0.31	
(110)1:1	1869.36	-4.02±0.93	-6.92±0.64	+0.44±0.92		0.04096±0.02221
(110)1:0	1905.90	-1.66±0.63		-1.09±1.57	+8.66±1.06	
(111)3:1	1286.93	-2.23±0.15	-7.73±0.17	-1.88±0.16	+3.83±0.17	0.12722±0.00743

Cu$_3$Pd

Face	σ	Δ^A_{12}	Δ^B_{12}	Δ^A_{23}	Δ^B_{23}	Ripple
(100)1:1	2341.92	-5.58±0.51	-6.83±0.62	+0.43±0.36		0.02328±0.02082
(100)1:0	2259.46	-7.17±0.51		-5.89±0.75	+1.32±0.62	
(110)1:1	2520.31	-8.21±1.01	-12.02±0.84	+2.30±1.38		0.04985±0.02419
(110)1:0	2517.05	-9.82±0.70		+1.34±2.28	-8.39±2.10	
(111)3:1	1793.00	+3.90±0.33	-0.83±0.41	+7.38±0.28	+11.27±0.54	0.10104±0.01576

Pd$_3$Cu

Face	σ	Δ^A_{12}	Δ^B_{12}	Δ^A_{23}	Δ^B_{23}	Ripple
(100)1:1	2438.15	-13.86±3.92	+0.48±0.41	+8.50±0.41		0.27452±0.08301
(100)1:0	1444.49	-11.47±0.33		+21.29±1.90	-4.06±0.45	0.21946±0.00637
(110)1:1	2103.89	-13.57±0.51	-9.44±0.65	+3.95±1.29		0.05583±0.01565
(110)1:0	2279.19	-21.51±0.97		+12.28±5.58	-5.05±1.29	
(111)3:1	1562.29	-9.95±0.27	-13.01±0.22	-6.37±0.19	-4.32±0.41	0.06775±0.01091

Cu$_3$Pt

Face	σ	Δ^A_{12}	Δ^B_{12}	Δ^A_{23}	Δ^B_{23}	Ripple
(100)1:1	2517.04	-6.33±0.40	+0.20±0.63	+1.28±0.34		0.12179±0.01928
(100)1:0	2279.98	+1.29±0.38		+8.87±0.41	+0.88±0.77	
(110)1:1	2935.31	-3.74±1.13	+0.17±1.28	+4.37±1.50		0.05154±0.03176
(110)1:0	2780.12	-7.29±0.73		+6.97±1.46	-2.31±0.92	
(111)3:1	1928.91	+4.05±0.29	+10.56±0.47	+10.82±0.26	+1.68±0.72	0.14040±0.01644

Table 11: Surface energies (in ergs/cm^2), planar relaxations (as percentages of the rigid interplanar spacing, see text) of the top two layers of several low-index faces of the L1$_2$ ordered structure. Δ^X_{ij} represents the relaxation between planes i and j of an atom of species X in layer i. The last column indicates the difference in position (in Å) of an atom A and an atom B in the top layer.

32

Pt_3Cu

Face	σ	Δ_{12}^A	Δ_{12}^B	Δ_{23}^A	Δ_{23}^B	Ripple
(100)1:1	2002.83	-6.12±0.35	-7.70±0.31	-3.00±0.25		0.03136±0.01323
(100)1:0	1924.84	-7.43±0.17		-3.97±0.26	-2.26±0.31	
(110)1:1	2101.70	-7.85±0.44	-7.63±0.52	-5.04±0.65		0.00320±0.01364
(110)1:0	2583.47					
(111)3:1	1146.30	-4.63±0.10	-8.61±0.15	-3.27±0.15	+1.51±0.12	0.09149±0.00587

Al_3Ni

Face	σ	Δ_{12}^A	Δ_{12}^B	Δ_{23}^A	Δ_{23}^B	Ripple
(100)1:1	3435.00	+5.31±2.02	-6.17±0.44	+1.57±0.43		0.21925±0.04706
(100)1:0	393.62	-0.39±0.14		+1.71±0.39	+7.64±0.15	
(110)1:1	2755.35	-11.72±0.82	-11.15±0.67	-1.65±1.33		0.00765±0.01948
(110)1:0	2260.07	-1.42±0.86		-10.55±1.07	+15.64±0.94	
(111)3:1	2410.59	-8.04±0.19	-12.99±0.19	-6.14±0.16	-1.34±0.23	0.10936±0.00853

Ni_3Al

Face	σ	Δ_{12}^A	Δ_{12}^B	Δ_{23}^A	Δ_{23}^B	Ripple
(100)1:1	2887.57	-5.46±0.48	+1.12±1.29	+1.30±0.45	+0.00±0.00	0.11819±0.03170
(100)1:0	3156.69	-0.54±0.49		+5.94±0.56	+0.66±1.14	
(110)1:1	3169.63	-7.17±1.24	-3.00±2.26	+0.29±2.34		0.05310±0.04449
(110)1:0	3885.99	-7.98±0.79		+3.08±1.92	-1.40±2.16	
(111)3:1	2575.54	+5.08±0.39	+13.05±1.18	+11.07±0.38	+2.34±1.13	0.16545±0.03266

Ag_3Au

Face	σ	Δ_{12}^A	Δ_{12}^B	Δ_{23}^A	Δ_{23}^B	Ripple
(100)1:1	1537.59	-20.70±3.46	-6.07±0.43	-2.21±0.41		0.30075±0.07993
(100)1:0	1488.54	-5.35±0.49		+13.85±2.92	-2.03±0.58	
(110)1:1	1661.68	-6.71±0.75	-5.16±0.72	+0.81±1.37		0.02262±0.02136
(110)1:0	1620.23	-11.38±1.04		+2.68±5.09	-3.43±1.15	
(111)3:1	1214.65	-4.29±0.35	-4.84±0.28	-1.74±0.27	-1.89±0.43	0.01303±0.01484

Au_3Ag

Face	σ	Δ_{12}^A	Δ_{12}^B	Δ_{23}^A	Δ_{23}^B	Ripple
(100)1:1	1578.82	-4.29±0.40	-4.27±0.58	-1.04±0.34		0.00036±0.02005
(100)1:0	1513.15	-5.14±0.27		-2.19±0.44	-1.21±0.48	0.10575±0.00563
(110)1:1	1618.62	-5.90±0.68	-6.50±0.78	-1.29±1.39		0.00869±0.02118
(110)1:0	1657.45	-5.61±0.42		-0.67±1.47	-0.94±1.80	
(111)3:1	1204.88	-3.85±0.25	-5.14±0.43	-1.50±0.27	-0.42±0.52	0.03046±0.01622

Table 11 (Cont'd)

33

Au$_3$Pd

Face	σ	Δ^A_{12}	Δ^B_{12}	Δ^A_{23}	Δ^B_{23}	Ripple
(100)1:1	2301.77	-1.57±0.71	-3.06±0.72	+0.06±0.50		0.03019±0.02910
(100)1:0	1458.72	-2.88±0.34		-0.52±0.46	+0.29±0.53	
(110)1:1	2138.84	-4.37±0.97	-5.38±1.07	-0.17±1.25		0.01437±0.02922
(110)1:0	1987.39	-3.85±0.66		-0.56±1.65	+1.01±1.85	
(111)3:1	1838.26	-3.48±0.36	-5.26±0.50	-1.66±0.31	-0.73±0.69	0.04182±0.02015

Pd$_3$Au

Face	σ	Δ^A_{12}	Δ^B_{12}	Δ^A_{23}	Δ^B_{23}	Ripple
(100)1:1	1584.61	-26.59±2.83	-1.02±0.60	+1.26±0.57		0.50770±0.06809
(100)1:0	2304.90	-3.22±0.72		+14.53±3.37	-1.12±0.71	0.06392±0.01425
(110)1:1	2104.72	-4.79±1.16	-2.88±1.17	+0.93±1.67		0.02681±0.03276
(110)1:0	2318.14	-10.22±1.26		+7.92±5.15	-2.94±1.10	
(111)3:1	1357.94	-0.60±0.56	+7.46±0.44	+8.77±0.44	-0.19±0.52	0.18482±0.02292

Ni$_3$Pd

Face	σ	Δ^A_{12}	Δ^B_{12}	Δ^A_{23}	Δ^B_{23}	Ripple
(100)1:1	2024.79	-10.92±0.33	-10.02±0.55	-3.98±0.31		0.01657±0.01635
(100)1:0	2513.61	-9.24±0.36		-7.63±0.42	+0.40±0.44	
(110)1:1	2477.88	-9.20±0.68	-13.05±0.56	+3.19±0.98		0.04994±0.01607
(110)1:0	2590.59	-10.89±0.45		+2.92±1.48	-11.72±0.89	
(111)3:1	1409.58	+1.72±0.20	+1.38±0.38	+8.36±0.15	-9.49±0.26	0.00714±0.01237

Pd$_3$Ni

Face	σ	Δ^A_{12}	Δ^B_{12}	Δ^A_{23}	Δ^B_{23}	Ripple
(100)1:1	1966.28	-19.69±3.37	-16.82±0.26	-8.30±0.21		0.05543±0.06985
(100)1:0	1240.30	-12.43±0.23		+18.09±1.83	-4.90±0.35	
(110)1:1	1882.18	-13.90±0.31	-11.39±0.36	+0.89±0.98		0.03418±0.00922
(110)1:0	1809.03	-22.77±0.67		-13.57±0.38	-6.29±1.06	
(111)3:1	617.93	-10.77±0.13	-14.22±0.09	-7.07±0.07	-4.99±0.24	0.07678±0.00483

Ni$_3$Pt

Face	σ	Δ^A_{12}	Δ^B_{12}	Δ^A_{23}	Δ^B_{23}	Ripple
(100)1:1	2577.37	-9.03±0.29	-1.81±0.62	-0.66±0.26		0.13363±0.01679
(100)1:0	2759.94	-0.46±0.29		+7.99±0.30	-0.30±0.71	
(110)1:1	3355.64	-4.79±0.77	+3.49±1.32	+8.72±1.08		0.10835±0.02736
(110)1:0	3234.27	-9.83±0.48		+5.24±1.25	-3.53±0.79	
(111)3:1	2042.79	+3.67±0.20	+11.18±0.49	+11.22±0.19	+1.36±0.68	0.16040±0.01477

Table 11: (Cont'd)

Pt$_3$Ni

Face	σ	Δ_{12}^A	Δ_{12}^B	Δ_{23}^A	Δ_{23}^B	Ripple
(100)1:1	2885.91	-1.61±0.69	-5.80±0.38	-0.70±0.34		0.08166±0.02087
(100)1:0	2100.63	-3.55±0.23		-1.47±0.41	+1.63±0.32	
(110)1:1	2701.88	-5.55±0.73	-7.38±0.60	-0.44±0.98		0.02527±0.01832
(110)1:0	2955.02	-3.42±0.60		-2.93±1.42	+6.98±1.14	
(111)3:1	1823.75	-3.18±0.15	-8.05±0.18	-2.37±0.16	+2.84±0.17	0.10961±0.00736

Table 11(Cont'd)
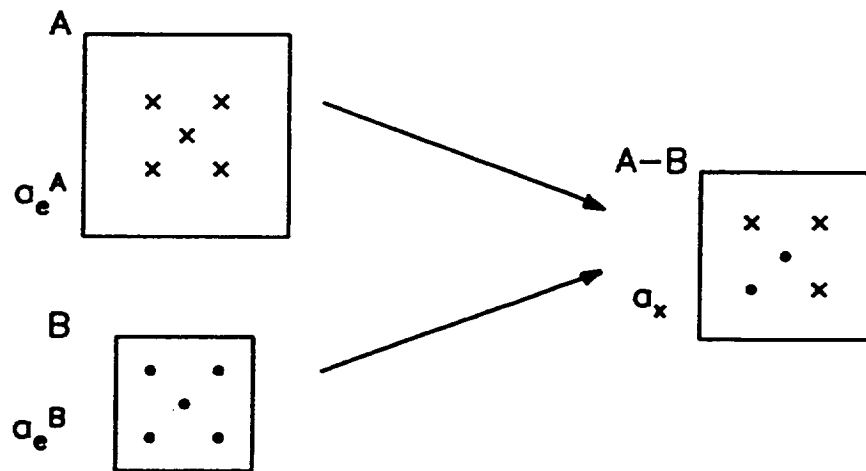
Fig. 1 : Ideal process of alloy formation.
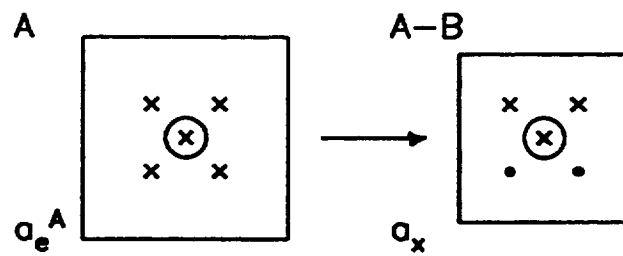
Fig. 2 : Transformation seen by an atom ($\otimes$) during the ideal process of alloy formation
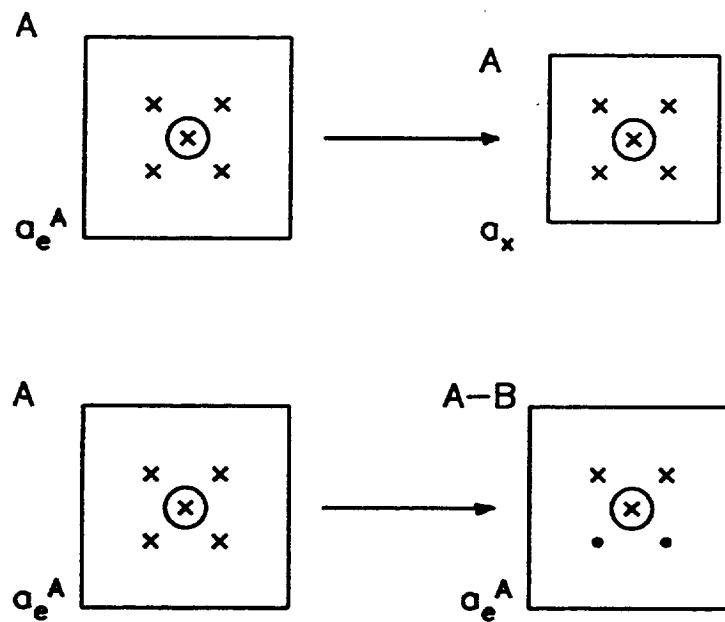
Fig. 3: Breakup of transformation shown in fig. 2 into two independent processes: (a) strain energy and (b) chemical energy. The dots indicate atoms of species B while X indicates atoms of species A. $\otimes$ indicates the reference atom.
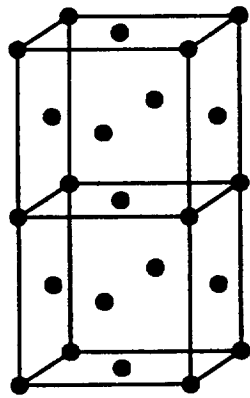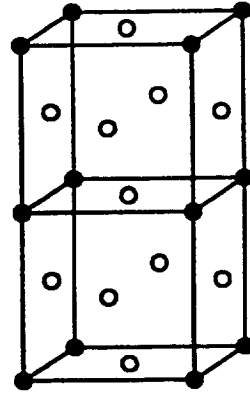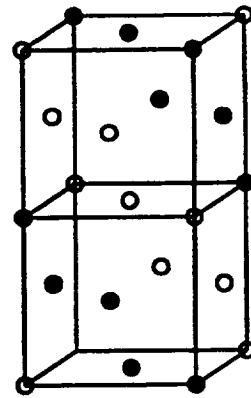
A_1 (A)　　　　　　$L1_2$ (AB_3)
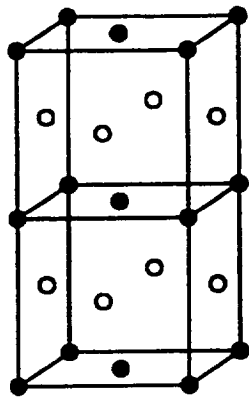
$L1_0$ (AB)　　　　　　$L1_1$ (AB)

Fig. 4: Ordered structures of fcc based alloys.

REPORT DOCUMENTATION PAGE

Public reporting burden for this collection of information is estimated to average 1 hour per response, including the time for reviewing instructions, searching existing data sources, gathering and maintaining the data needed, and completing and reviewing the collection of information. Send comments regarding this burden estimate or any other aspect of this collection of information, including suggestions for reducing this burden, to Washington Headquarters Services, Directorate for Information Operations and Reports, 1215 Jefferson Davis Highway, Suite 1204, Arlington, VA 22202-4302, and to the Office of Management and Budget, Paperwork Reduction Project (0704-0188), Washington, DC 20503.

1. AGENCY USE ONLY (Leave blank)	2. REPORT DATE	3. REPORT TYPE AND DATES COVERED
	July 1994	Technical Memorandum

4. TITLE AND SUBTITLE

Modelling of Surfaces

Part II–Metallic Alloy Surfaces Using the BFS Method

5. FUNDING NUMBERS

WU–505–90–53

6. AUTHOR(S)

Guillermo Bozzolo, John Ferrante, and Robert J. Kobistek

7. PERFORMING ORGANIZATION NAME(S) AND ADDRESS(ES)

National Aeronautics and Space Administration
Lewis Research Center
Cleveland, Ohio 44135–3191

8. PERFORMING ORGANIZATION REPORT NUMBER

E–9011

9. SPONSORING/MONITORING AGENCY NAME(S) AND ADDRESS(ES)

National Aeronautics and Space Administration
Washington, D.C. 20546–0001

10. SPONSORING/MONITORING AGENCY REPORT NUMBER

NASA TM–106675

11. SUPPLEMENTARY NOTES

12a. DISTRIBUTION/AVAILABILITY STATEMENT

Unclassified - Unlimited
Subject Categories 76 and 26

12b. DISTRIBUTION CODE

13. ABSTRACT (Maximum 200 words)

Using BFS, a new semiempirical method for alloys, we study the surface structure of fcc ordered binary alloys. We concentrate on the calculation of surface energies and surface relaxations for the $L1_0$ and $L1_2$ ordered structures. Different terminations of the low-index faces are studied. Also, we present results for the interlayer relaxations for planes close to the surface, revealing different relaxations for atoms of different species producing a rippled surface layer.

14. SUBJECT TERMS

Alloys; Semiempirical methods; Metallic surfaces

15. NUMBER OF PAGES
41

16. PRICE CODE
A03

17. SECURITY CLASSIFICATION OF REPORT	18. SECURITY CLASSIFICATION OF THIS PAGE	19. SECURITY CLASSIFICATION OF ABSTRACT	20. LIMITATION OF ABSTRACT
Unclassified	Unclassified	Unclassified	

NSN 7540-01-280-5500